Letter

Superconductivity in Li_8Au electride

Xiaohua Zhang,[1] Yansun Yao,[2,*] Shicong Ding,[1] Aitor Bergara,[3,4,5] Fei Li,[1] Yong Liu,[1] Xiang-Feng Zhou,[1,6] and Guochun Yang[1,†]

[1]*State Key Laboratory of Metastable Materials Science and Technology and Key Laboratory for Microstructural Material Physics of Hebei Province, School of Science, Yanshan University, Qinhuangdao 066004, China*

[2]*Department of Physics and Engineering Physics, University of Saskatchewan, Saskatoon, Saskatchewan, Canada S7N 5E2*

[3]*Departamento de Física, Universidad del País Vasco-Euskal Herriko Unibertsitatea, UPV/EHU, 48080 Bilbao, Spain*

[4]*Donostia International Physics Center (DIPC), 20018 Donostia, Spain*

[5]*Centro de Física de Materiales CFM, Centro Mixto CSIC-UPV/EHU, 20018 Donostia, Spain*

[6]*Center for High Pressure Science (CHiPS), State Key Laboratory of Metastable Materials Science and Technology, Yanshan University, Qinhuangdao 066004, China*

(Received 7 October 2022; revised 19 December 2022; accepted 27 February 2023; published 10 March 2023)

Located at crystal voids, interstitial anion electrons (IAEs) have diverse topologies, which may be tuned to achieve different properties. Elucidating the role of IAEs in electron-phonon coupling (EPC), and using it to design electride superconductors, leads to the current prediction of superconducting Li_8Au at high pressure. We suggest that the occurence of high-temperature superconductivity in electrides requires high-symmetry structures with hydrogenlike cages, an electron acceptor element to balance charges, and isolated IAEs coupled with medium-frequency vibrations. The uniquely designed Li_8Au electride has a NaCl-type ($B1$) lattice, with atomic Au and cubic Li_8 cages as bases. Isolated IAEs are formed at the cage centers, with extra charges taken up by Au. These octahedrally coordinated IAEs have a p-orbital-like attribute and are strongly coupled with atomic vibrations in the Li_8 cages. The strong EPC in Li_8Au results in a calculated T_c of 73.1 K at 250 GPa, which is the highest T_c reported to date for all the electrides. A slight substitutional Pt doping can enhance the T_c of Li_8Au to exceed liquid nitrogen temperature.

DOI: 10.1103/PhysRevB.107.L100501

The search for new superconductors is of great interest in condensed matter physics. Over the years, several types of BCS superconductors have been discovered, from earlier $A15$-type Nb_3Ge [1], layer-type MgB_2 [2], to recent perovskite-type H_3S [3], and sodalite-type LaH_{10} [4,5]. The discovered T_c in BCS superconductors grows continuously from the previously thought upper limit around 40 K ("McMillan limit") to above 260 K in recently discovered hydrides [5,6]. Interestingly, high-T_c hydrides tend to have high symmetry structures, which has played a guiding role in the search for new superconductors [7,8].

The co-occurrence of superconducting and electride states is less explored. In electrides, a fraction of electrons break away from atoms to reside in the interstitial voids, behaving like nucleus-free anions [interstitial anion electrons (IAEs)] [9], which can be tuned in magnitude and topology [10–12] to achieve new properties. Alkali metals become electrides under high pressure [13,14] and exhibit moderate superconductivity ($T_c < 20$ K) [15,16]. Incorporating nonmetal elements into the electrides can modulate the IAEs and enhance superconductivity. For example, Li_5C [17], Li_5N [18], and Li_6P [19] present interconnected IAEs which enhance the T_c to 48.3, 48.97, and 39.3 K, respectively.

High-T_c hydrides tend to favor high-symmetry configurations of hydrogen (H), e.g., H_8 [20], H_{24} [21], and H_{32} [22] cages. One approach to turn these cages into high-symmetry electrides is to replace H by elements with same valence configuration but more electropositive [23,24]. Lithium (Li) is an obvious option, since it behaves like H at high pressure and maintains electride states that favor superconductivity (Fig. 1) [15,25]. In addition, Li has the ability to form clusters of various stoichiometries ("superatoms") when alloyed with some transition metals [26]. The formation of electrides generally requires that Li has a higher stoichiometric ratio than the other metal [27]. Therefore, the stabilization of high symmetry electrides of Li requires selecting an electron acceptor to satisfy geometry and charge balance. Among the elements, gold (Au) stands out due to its unique chemical attributes and the ability to present high oxidation states at high pressure (Fig. 1) [28–30]. As a host, Au also presents a possibility of stabilizing Li-Au electrides [31].

In this Letter, we report a Li_8Au electride with good superconducvitiy. The structure was inspired by previously reported Li_3Au, in which Au and edge shared bcc Li_3 occupy two fcc sites in a NaCl lattice [Fig. 2(b)]. In Li_8Au, we kept the NaCl motif, but replaced the Li_3 with cubic Li_8 cages, isostructural to the H_8 cages [20,32–34]. IAEs are formed at the centers of the Li_8 cages, and arranged in another fcc sublattice. The strong electron-phonon coupling (EPC) in Li_8Au induces a high T_c of ~ 73.1 K at 250 GPa, much higher than in previously reported electrides.

*yansun.yao@usask.ca
†yanggc468@nenu.edu.cn

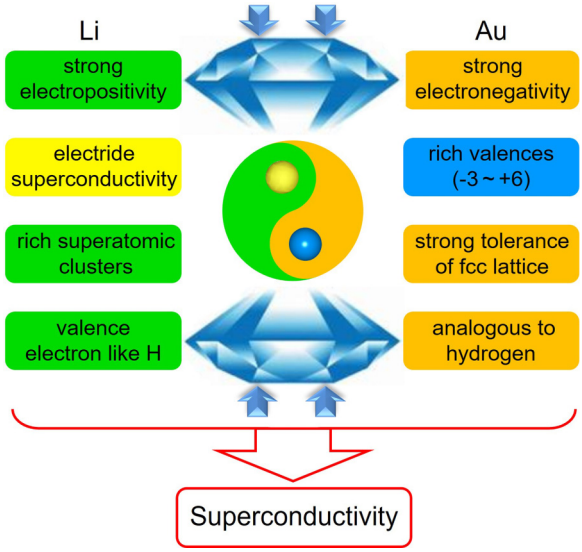

FIG. 1. Schematic illustration of the design strategy for superconducting electrides consisting of Li and Au. The special features of Li and Au that occur under high pressure are highlighted in yellow and blue, respectively.

Hydrogen cages are important intermediate structures between molecular H_2 and atomic H, which, after being precompressed by metal atoms, contribute enormously to the EPC. Simple-cubic (sc) H_8 is a common H cage [20,22] observed in hydrides [Fig. 2(a)]. Considering the similarity between Li and H, the formation of a cubic Li_8 cage should be possible, but it would require weaker bonds, which means that some valence electrons need to be removed from the cage. The cubic voids naturally accommodate the extra electrons, forming IAEs [Fig. 2(a)]. It should be noted that the crystalline counterpart of simple cubic is dynamically unstable, and even less so at high pressures when Li departs from nearly free electron behavior (Fig. S1 of the Supplemental Material [35]). At high pressure, the reduced interstitial sites in crystalline simple cubic could not store sufficient IAEs required to stabilize the structure, and therefore elemental Li must adopt other structures [15]. Au is a suitable candidate for an additional "electron reservoir" in the crystal due to its exceptional charge adjustability, which can act as both an electron donor and an acceptor [28,31]. Furthermore, the fcc sublattice of Au is robust to neighboring superatoms (Fig. S2 [35]), ideal for hosting sc Li_8 in the crystal.

We replace the edge-sharing bcc units in Li_3Au with IAEs-centered Li_8 units. This results in a stoichiometric Li_8Au within the same Fm-3m space group [Fig. 2(c)]. The IAE has a smaller volume than Li atom (Table S1 [35]), which means that at high pressure the IAE-centered cubic unit is energetically more favorable than its atom-centered counterpart. Indeed, the convex hull of the Li-Au phase diagram indicates that Li_8Au will replace Li_3Au to become thermodynamically stable at high pressure (above 177.3 GPa) (Fig. S3). Furthermore, Fm-3m Li_8Au becomes dynamically stable in the pressure range 120–300 GPa (Fig. S4) as confirmed by phonon calculations. All computational details can be found in the Supplemental Material [35].

The stability of Li_8Au is enhanced by charge-transfer-induced ionic interaction. The Li_8 cage loses a total charge of $5.24e^-$ to the surroundings. The two electron acceptors, the IAE and Au atom, gain $0.74e^-$ and $4.50e^-$ [Fig. 2(c)], respectively. Thus, the IAE-centered Li_8 is positively charged, behaving as a superatomic cation. The electrons transferred to the Au atom must populate its 6p orbitals (details below), which causes the expansion of its atomic radius, allowing a larger space to accommodate IAE-centered Li_8. In addition,

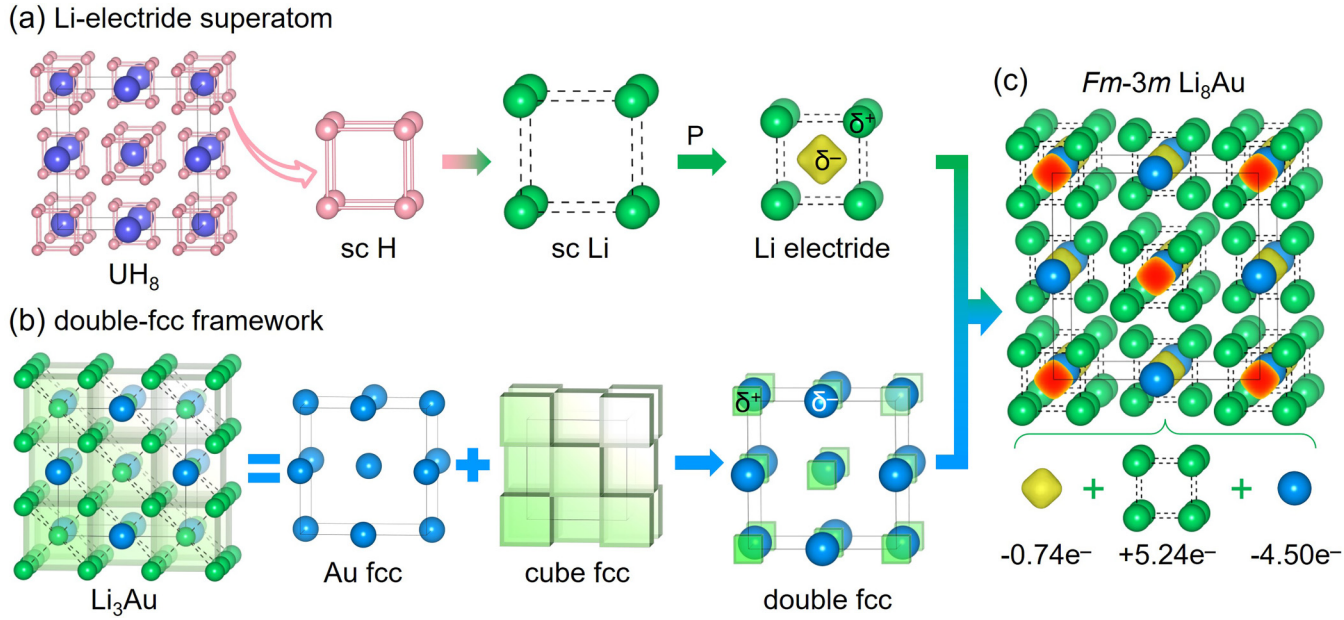

FIG. 2. (a) Cubic Li electride superatom analogous to the H_8 cage in UH_8. (b) The NaCl lattice in Li_3Au consisting of Li_3 and Au bases. (c) Crystal structure of Fm-3m Li_8Au. The IAEs are shown by yellow spots. Numbers below identities are the calculated Bader charges of their constitutional units at 200 GPa (+/− indicates electronic loss/gain).

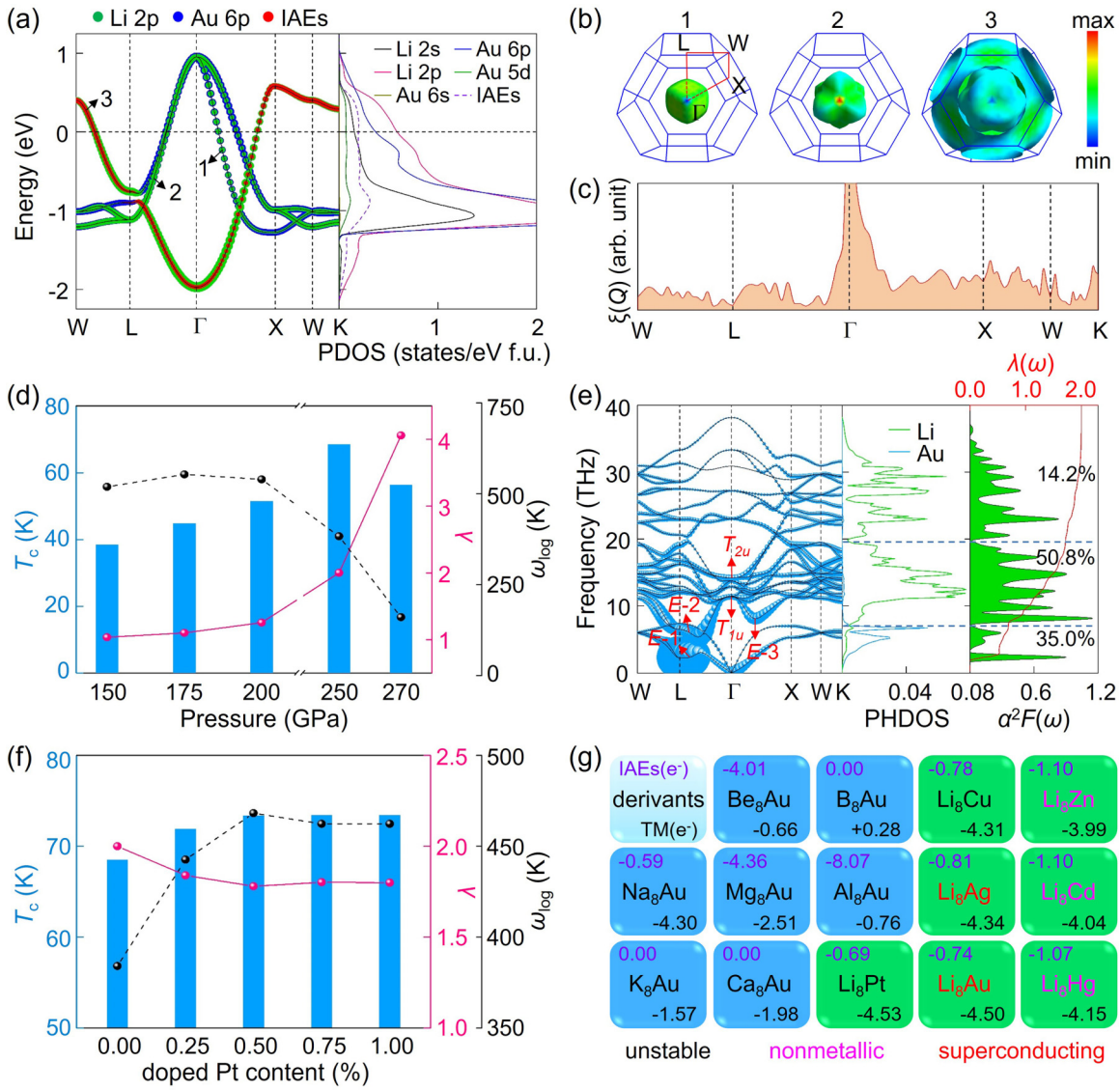

FIG. 3. (a) Orbital-projected electronic bands and density of states (DOS). (b) Fermi surfaces corresponding to the three bands crossing the E_F, color coded by the Fermi velocity. (c) The nesting function $\xi(Q)$ along high-symmetry paths. (d) Calculated λ, ω_{log}, and T_c of Li_8Au at different pressures. (e) Phonon dispersion relations, projected phonon density of states (PHDOS), Eliashberg spectral function $\alpha^2F(\omega)$, and frequency-dependent EPC parameter $\lambda(\omega)$. The size of solid dots on the phonon spectra signifies the contribution to the EPC ($\lambda_{q,v}$). (f) The evolution of λ, ω_{log}, and T_c of Pt-doped Li_8Au with increasing Pt content at 250 GPa. (g) Derivatives of Li_8Au substituting Li or Au with their neighboring elements. Dynamically unstable structures are marked in black and stable ones in color. The values represent the calculated Bader charges of IAEs (purple) and En atoms (black) at 200 GPa.

the Li-Li bond interaction in IAE-centered Li_8 (Fig. S5), induced by electron transfer, also contributes to the stability of Li_8Au.

Li_8Au presents regular IAEs in a high-symmetry metallic structure. The electronic band structure shows three bands crossing the Fermi level (E_F), mainly contributed by Li $2p$, Au $6p$, and IAEs [Fig. 3(a)]. These bands feature a simultaneous occurrence of flat bands (W-L, X-W-K paths) and steep bands (W-L-Γ-X paths). The three corresponding Fermi surfaces (FSs) are shown in Fig. 3(b). Both FSs 1 and 2 are derived mainly from a mixture of Li $2p$ and Au $6p$ states, while FS 3 is primarily from the hybridized states of Li $2p$ and IAEs, and hybridized states of Li $2p$ and Au $6p$. This indicates that Li $2p$ acts as a common channel interacting with all other states. Based on the orbital hybridization, the IAE's octahedral topology, and the orbital symmetry matching rule, we infer that IAEs in Li_8Au show a p-orbital-like attribute (Fig. S6). The maximum Fermi velocity is concentrated at two centrosymmetric points on the FS 2, whereas the medium and low Fermi velocities have a symmetrical distribution on all three FSs [Fig. 3(b)], indicating strong FS nesting [54]. The nesting function $\xi(Q)$ shows that a considerable region of the FS is nested by Γ-X-W-K vectors [Fig. 3(c)] [55]. Moreover, a sharp van Hove singularity (VHS) occurs at -1.09 eV below the E_F (Fig. S7), similar to H_3S [56,57] and LaH_{10} [58]. These electronic structures have been shown to be favorable for the formation of stable Cooper pairs [17,59].

The superconductivity of Li_8Au is evaluated via EPC calculations and the Allen-Dynes modified McMillan formula [60,61]. As shown in Fig. 3(d), the EPC constant λ increases notably between 150 and 270 GPa, mainly due to the softening of acoustic branches around the L point and the low-energy optical branches around L and the Γ-X path [Figs. 3(e) and S8]. However, the phonon frequency logarithmic average $\omega_{\log}$ decreases with pressure. The two competing mechanisms result in a T_c peaking at 250 GPa. Using a Coulomb pseudopotential of $\mu^* = 0.1$, the calculated T_c at 250 GPa is 68.5 K [Fig. 3(d) and Table S2], and considering its semiempirical character [62], the estimate of T_c when μ^* is in the range 0.08–0.13 goes between 73.1 and 62.2 K (Fig. S9). With inclusion of spin-orbital coupling, the T_c of Li_8Au is calculated to be 66.3 K with $\mu^* = 0.1$ (Fig. S10). All these T_c values exceed the highest T_c reported to date for electrides [48.3 K for Li_5C [17], 48.97 K for Li_5N [18] and others (Fig. S11)], as well as higher than the T_c of Au compounds [$\sim$ 30 K for $Ba(AuH_2)_2$ [63]]. Moreover, Li_8Au is predicted to be a single-gap superconductor, corresponding to a T_c of 81.8 K (Fig. S12) based on electron-phonon Wannier calculations [64]. Given a sharp DOS peak (VHS) below the E_F in Li_8Au, replacing a small amount of Au with Pt, acting as a hole donor, might boost N_{E_F} to yield higher T_c. Using virtual crystal approximation [65], an optimal T_c value of 78.3 K (with $\mu^* = 0.1$) is achieved at Pt doping close to 0.5% [Figs. 3(f) and S13–S15]. For superconductors with light mass elements such as hydrides, the nuclear quantum effect (NQE) may have effects on the T_c [66–68]. However, the NQE has been shown to have neglectable effects on superconducting Li [69] and is therefore not included in the superconductivity study of Li_8Au.

The PHDOS and Eliashberg spectral function $\alpha^2F(\omega)$ can be divided into three regions: the low-frequency region (below 7 THz) dominated by the Au atom, the Li_8 cage-derived intermediate-frequency region (7–20 THz), and the high-frequency (above 20 THz) region [Fig. 3(e)], which make the contribution of 35.0%, 50.8%, and 14.2% total λ, respectively. The strongest local EPC is from two softened acoustic modes around the L point [Fig. 3(e)], i.e., the twofold degenerate E-1 and E-2 modes. These modes represent stretching vibrations of pairs of Li atoms across the body diagonal in the Li_8 cage, which favors a strong extrusion interaction with IAEs (Fig. S16). Meanwhile, the Au atom also participates in the vibrations, exhibiting a low-frequency feature. These two modes induce a shift in energy around the L point, and a removal of degeneracy around the Γ point (Fig. S17). The mechanism by which the E-1 and E-2 modes promote the EPC is similar to that of the E_{2g} mode in MgB_2 [70]. In the intermediate-frequency region, the three modes (T_{1u}, T_{2u}, and soft E-3) associated with twisting vibrations of the Li_8 cage (Fig. S18) induce a minor shift of the flat bands along the W-L and X-W-K paths (Fig. S19). Therefore, the Li_8 cage and IAEs dominate superconductivity in Li_8Au.

Finally, we explore the key factors for stabilizing this electride using elemental substitutions for Li and Au [Fig. 3(g)]. For clarity, the electropositive atoms (replacing Li) are denoted by Ep, and the electronegative ones (replacing Au) are En. It turns out that no Ep_8Au, apart from Li_8Au, is dynamically stable [Figs. S20 and S21 and Fig. 3(g)]. Li_8En, on the other hand, has several dynamical stable structures, e.g., Li_8Ag, Li_8Zn, Li_8Cd, and Li_8Hg, which shows robustness to electronegative replacement [Fig. 3(g) and Figs. S22 and S23]. Interestingly, Li_8Ag is metallic (Figs. S24 and S25), while Li_8Zn, Li_8Cd, and Li_8Hg are all semiconducting (Fig. S26). This suggests that electronic properties in the double-fcc electride can be further tuned through isotypic replacement or doping.

In summary, we have designed an electride material, Li_8Au, consisting of a double fcc lattice with atomic Au and cubic Li_8 cages as bases. The IAEs are located at the cage centers, forming octahedronlike IAEs with a p-orbital-type attribute. This topology of the IAEs induces strong coupling to the vibration of Li_8 cages, and enhances the phonon mediated superconductivity. Li_8Au is calculated to have the highest superconducting T_c among all reported electrides to date. Moreover, the T_c of Li_8Au can be further increased by substitutional Pt doping. Our work serves as a guide to design superconducting electrides with high-symmetry building blocks.

This work was supported by the National Key Research and Development Program of China (Grant No. 2022YFA1402300), the Natural Science Foundation of China under Grants No. 52025026, No. 21873017, and No. 21573037, the Postdoctoral Science Foundation of China under Grant No. 2013M541283, the Innovation Capability Improvement Project of Hebei province (Grant No. 22567605H), the Natural Science Foundation of Hebei Province (Grant No. B2021203030), Science and Technology Project of Hebei Education Department (Grants No. JZX2023020 and No. QN2023246), and Natural Sciences and Engineering Research Council of Canada (NSERC). A.B. acknowledges financial support from the Spanish Ministry of Science and Innovation (Grant No. PID2019-105488GB-I00) and the Department of Education, Universities and Research of the Basque Government and the University of the Basque Country (Grant No. IT1707-22).

[1] B. T. Matthias, T. H. Geballe, R. H. Willens, E. Corenzwit, and G. W. Hull, Superconductivity of Nb_3Ge, Phys. Rev. **139**, A1501 (1965).

[2] J. Nagamatsu, N. Nakagawa, T. Muranaka, Y. Zenitani, and J. Akimitsu, Superconductivity at 39 K in magnesium diboride, Nature (London) **410**, 63 (2001).

[3] A. P. Drozdov, M. I. Eremets, I. A. Troyan, V. Ksenofontov, and S. I. Shylin, Conventional superconductivity at 203 kelvin at high pressures in the sulfur hydride system, Nature (London) **525**, 73 (2015).

[4] A. P. Drozdov, P. P. Kong, V. S. Minkov, S. P. Besedin, M. A. Kuzovnikov, S. Mozaffari, L. Balicas, F. F. Balakirev, D. E. Graf, V. B. Prakapenka, E. Greenberg, D. A. Knyazev, M. Tkacz, and M. I. Eremets, Superconductivity at 250 K in lanthanum hydride under high pressures, Nature (London) **569**, 528 (2019).

[5] M. Somayazulu, M. Ahart, A. K. Mishra, Z. M. Geballe, M. Baldini, Y. Meng, V. V. Struzhkin, and R. J. Hemley, Evidence for Superconductivity above 260 K in Lanthanum Superhydride at Megabar Pressures, Phys. Rev. Lett. **122**, 027001 (2019).

[6] E. Snider, N. Dasenbrock-Gammon, R. McBride, X. Wang, N. Meyers, K. V. Lawler, E. Zurek, A. Salamat, and R. P. Dias, Synthesis of Yttrium Superhydride Superconductor with a Transition Temperature up to 262 K by Catalytic Hydrogenation at High Pressures, Phys. Rev. Lett. **126**, 117003 (2021).

[7] H. Xie, Y. Yao, X. Feng, D. Duan, H. Song, Z. Zhang, S. Jiang, S. A. T. Redfern, V. Z. Kresin, C. J. Pickard, and T. Cui, Hydrogen Pentagraphenelike Structure Stabilized by Hafnium: A High-Temperature Conventional Superconductor, Phys. Rev. Lett. **125**, 217001 (2020).

[8] Y. Sun, J. Lv, Y. Xie, H. Liu, and Y. Ma, Route to a Superconducting Phase above Room Temperature in Electron-Doped Hydride Compounds under High Pressure, Phys. Rev. Lett. **123**, 097001 (2019).

[9] M.-S. Miao and R. Hoffmann, High pressure electrides: A predictive chemical and physical theory, Acc. Chem. Res. **47**, 1311 (2014).

[10] Y. Zhang, W. Wu, Y. Wang, S. A. Yang, and Y. Ma, Pressure-stabilized semiconducting electrides in alkaline-earth-metal subnitrides, J. Am. Chem. Soc. **139**, 13798 (2017).

[11] H. Hosono and M. Kitano, Advances in materials and applications of inorganic electrides, Chem. Rev. **121**, 3121 (2021).

[12] Y. Ma, M. Eremets, A. R. Oganov, Y. Xie, I. Trojan, S. Medvedev, A. O. Lyakhov, M. Valle, and V. Prakapenka, Transparent dense sodium, Nature (London) **458**, 182 (2009).

[13] A. Bergara, J. B. Neaton, and N. W. Ashcroft, Pairing, π-bonding, and the role of nonlocality in a dense lithium monolayer, Phys. Rev. B **62**, 8494 (2000).

[14] A. Rodriguez-Prieto and A. Bergara, Pressure induced complexity in a lithium monolayer: Ab initio calculations, Phys. Rev. B **72**, 125406 (2005).

[15] K. Shimizu, H. Ishikawa, D. Takao, T. Yagi, and K. Amaya, Superconductivity in compressed lithium at 20 K, Nature (London) **419**, 597 (2002).

[16] V. V. Struzhkin, M. I. Eremets, W. Gan, H.-k. Mao, and R. J. Hemley, Superconductivity in dense lithium, Science **298**, 1213 (2002).

[17] Z. S. Pereira, G. M. Faccin, and E. Z. da Silva, Predicted superconductivity in the electride Li_5C, J. Phys. Chem. C **125**, 8899 (2021).

[18] Z. Wan, C. Zhang, T. Yang, W. Xu, and R. Zhang, Predicted superconductivity and superionic state in the electride Li_5N under high pressure, New J. Phys. **24**, 113012 (2022).

[19] Z. Zhao, S. Zhang, T. Yu, H. Xu, A. Bergara, and G. Yang, Predicted Pressure-Induced Superconducting Transition in Electride Li_6P, Phys. Rev. Lett. **122**, 097002 (2019).

[20] I. A. Kruglov, A. G. Kvashnin, A. F. Goncharov, A. R. Oganov, S. S. Lobanov, N. Holtgrewe, S. Jiang, V. B. Prakapenka, E. Greenberg, and A. V. Yanilkin, Uranium polyhydrides at moderate pressures: Prediction, synthesis, and expected superconductivity, Sci. Adv. **4**, eaat9776 (2018).

[21] H. Wang, J. S. Tse, K. Tanaka, T. Iitaka, and Y. Ma, Superconductive sodalite-like clathrate calcium hydride at high pressures, Proc. Natl. Acad. Sci. USA **109**, 6463 (2012).

[22] H. Liu, I. I. Naumov, R. Hoffmann, N. W. Ashcroft, and R. J. Hemley, Potential high-T_c superconducting lanthanum and yttrium hydrides at high pressure, Proc. Natl. Acad. Sci. USA **114**, 6990 (2017).

[23] Z. Liu, Q. Zhuang, F. Tian, D. Duan, H. Song, Z. Zhang, F. Li, H. Li, D. Li, and T. Cui, Proposed Superconducting Electride Li_6C by Sp-Hybridized Cage States at Moderate Pressures, Phys. Rev. Lett. **127**, 157002 (2021).

[24] Y. Xie, A. R. Oganov, and Y. Ma, Novel High Pressure Structures and Superconductivity of $CaLi_2$, Phys. Rev. Lett. **104**, 177005 (2010).

[25] H. Hosono, S.-W. Kim, S. Matsuishi, S. Tanaka, A. Miyake, T. Kagayama, and K. Shimizu, Superconductivity in room-temperature stable electride and high-pressure phases of alkali metals, Philos. Trans. R. Soc. A **373**, 20140450 (2015).

[26] L. Yan, J. Liu, and J. Shao, Superatomic properties of transition-metal-doped tetrahexahedral lithium clusters: $TM@Li_{14}$, Mol. Phys. **118**, e1592256 (2020).

[27] X. Zhang, F. Li, A. Bergara, and G. Yang, Pressure-induced superconductivity in Li-Te electrides, Phys. Rev. B **104**, 134505 (2021).

[28] J. Lin, S. Zhang, W. Guan, G. Yang, and Y. Ma, Gold with +4 and +6 Oxidation States in AuF_4 and AuF_6, J. Am. Chem. Soc. **140**, 9545 (2018).

[29] S. Buckart, G. Ganteför, Y. D. Kim, and P. Jena, Anomalous behavior of atomic hydrogen interacting with gold clusters, J. Am. Chem. Soc. **125**, 14205 (2003).

[30] S. Furuseth, K. Selte, and A. Kjekshus, Redetermined crystal structures of $PdAs_2$, $PdSb_2$, PtP_2, $PtAs_2$, $PtSb_2$, α-$PtBi_2$, and $AuSb_2$, Acta Chem. Scand. **19**, 735 (1965).

[31] G. Yang, Y. Wang, F. Peng, A. Bergara, and Y. Ma, Gold as a 6p-element in dense lithium aurides, J. Am. Chem. Soc. **138**, 4046 (2016).

[32] Z. Zhang, T. Cui, M. J. Hutcheon, A. M. Shipley, H. Song, M. Du, V. Z. Kresin, D. Duan, C. J. Pickard, and Y. Yao, Design Principles for High-Temperature Superconductors with a Hydrogen-Based Alloy Backbone at Moderate Pressure, Phys. Rev. Lett. **128**, 047001 (2022).

[33] S. Di Cataldo, C. Heil, W. von der Linden, and L. Boeri, $LaBH_8$: Towards high-T_c low-pressure superconductivity in ternary superhydrides, Phys. Rev. B **104**, L020511 (2021).

[34] X. Liang, A. Bergara, X. Wei, X. Song, L. Wang, R. Sun, H. Liu, R. J. Hemley, L. Wang, G. Gao, and Y. Tian, Prediction of high-T_c superconductivity in ternary lanthanum borohydrides, Phys. Rev. B **104**, 134501 (2021).

[35] See Supplemental Material at http://link.aps.org/supplemental/10.1103/PhysRevB.107.L100501 for computational details, crystal structures, electron localization functions, phonon dispersion relations, convex hull of Li-Au phases, electronic band structures, Eliashberg spectral function and frequency-dependent EPC parameter, estimated Tc's, density of states and superconducting gaps, visualization of vibrational modes, and supplemental tables (includes Refs. [36–53]).

[36] Y. Wang, J. Lv, L. Zhu, and Y. Ma, Crystal structure prediction via particle-swarm optimization, Phys. Rev. B **82**, 094116 (2010).

[37] G. Kresse and J. Furthmüller, Efficient iterative schemes for ab initio total-energy calculations using a plane-wave basis set, Phys. Rev. B **54**, 11169 (1996).

[38] J. P. Perdew, K. Burke, and M. Ernzerhof, Generalized Gradient Approximation Made Simple, Phys. Rev. Lett. **77**, 3865 (1996).

[39] P. E. Blöchl, Projector augmented-wave method, Phys. Rev. B **50**, 17953 (1994).

[40] P. Blaha, K. Schwarz, P. Sorantin, and S. B. Trickey, Full-potential, linearized augmented plane wave programs for crystalline systems, Comput. Phys. Commun. **59**, 399 (1990).

[41] P. Giannozzi, S. Baroni, N. Bonini, M. Calandra, R. Car, C. Cavazzoni, D. Ceresoli, G. L. Chiarotti, M. Cococcioni, I. Dabo *et al.*, QUANTUM ESPRESSO: A modular and open-source software project for quantum simulations of materials, J. Phys.: Condens. Matter **21**, 395502 (2009).

[42] K. Lee, S. W. Kim, Y. Toda, S. Matsuishi, and H. Hosono, Dicalcium nitride as a two-dimensional electride with an anionic electron layer, Nature (London) **494**, 336 (2013).

[43] B. Sa, R. Xiong, C. Wen, Y.-L. Li, P. Lin, Q. Lin, M. Anpo, and Z. Sun, Electronic anisotropy and superconductivity in one-dimensional electride Ca_3Si, J. Phys. Chem. C **124**, 7683 (2020).

[44] X. Zhang, Y. Zhao, A. Bergara, and G. Yang, Superconducting $Li_{10}Se$ electride under pressure, J. Chem. Phys. **156**, 194112 (2022).

[45] C. Kokail, C. Heil, and L. Boeri, Search for high- T_c conventional superconductivity at megabar pressures in the lithium-sulfur system, Phys. Rev. B **94**, 060502(R) (2016).

[46] Q. Wang, W. Cui, K. Gao, J. Chen, T. Gu, M. Liu, J. Hao, J. Shi, and Y. Li, Pressure-stabilized superconducting electride Li_5C, Phys. Rev. B **106**, 054519 (2022).

[47] X. Li, A. Hermann, F. Peng, J. Lv, Y. Wang, H. Wang, and Y. Ma, Stable lithium argon compounds under high pressure, Sci. Rep. **5**, 16675 (2015).

[48] Z. Wan, W. Xu, T. Yang, and R. Zhang, As-Li electrides under high pressure: Superconductivity, plastic, and superionic states, Phys. Rev. B **106**, L060506 (2022).

[49] X. Wang, Y. Wang, J. Wang, S. Pan, Q. Lu, H.-T. Wang, D. Xing, and J. Sun, Pressure Stabilized Lithium-Aluminum Compounds with Both Superconducting and Superionic Behaviors, Phys. Rev. Lett. **129**, 246403 (2022).

[50] J.-Y. You, B. Gu, G. Su, and Y. P. Feng, Emergent Kagome electrides, J. Am. Chem. Soc. **144**, 5527 (2022).

[51] X. Liu, X. Huang, P. Song, C. Wang, L. Zhang, P. Lv, L. Liu, W. Zhang, J.-H. Cho, and Y. Jia, Strong electron-phonon coupling superconductivity in compressed α-MoB_2 induced by double Van Hove singularities, Phys. Rev. B **106**, 064507 (2022).

[52] X. Dong, A. R. Oganov, H. Cui, X.-F. Zhou, and H.-T. Wang, Electronegativity and chemical hardness of elements under pressure, Proc. Natl. Acad. Sci. USA **119**, e2117416119 (2022).

[53] A. Togo, F. Oba, and I. Tanaka, First-principles calculations of the ferroelastic transition between rutile-type and $CaCl_2$-type SiO_2 at high pressures, Phys. Rev. B **78**, 134106 (2008).

[54] T. Kiss, T. Yokoya, A. Chainani, S. Shin, T. Hanaguri, M. Nohara, and H. Takagi, Charge-order-maximized momentum-dependent superconductivity, Nat. Phys. **3**, 720 (2007).

[55] J. S. Tse, Y. Yao, and K. Tanaka, Novel Superconductivity in Metallic SnH_4 under High Pressure, Phys. Rev. Lett. **98**, 117004 (2007).

[56] W. Sano, T. Koretsune, T. Tadano, R. Akashi, and R. Arita, Effect of Van Hove singularities on high-T_c superconductivity in H_3S, Phys. Rev. B **93**, 094525 (2016).

[57] D. Duan, Y. Liu, F. Tian, D. Li, X. Huang, Z. Zhao, H. Yu, B. Liu, W. Tian, and T. Cui, Pressure-induced metallization of dense $(H_2S)_2H_2$ with high-T_c superconductivity, Sci. Rep. **4**, 6968 (2014).

[58] L. Liu, C. Wang, S. Yi, K. W. Kim, J. Kim, and J.-H. Cho, Microscopic mechanism of room-temperature superconductivity in compressed LaH_{10}, Phys. Rev. B **99**, 140501(R) (2019).

[59] C. Wang, S. Yi, and J.-H. Cho, Multiband nature of room-temperature superconductivity in LaH_{10} at high pressure, Phys. Rev. B **101**, 104506 (2020).

[60] R. C. Dynes, McMillan's equation and the Tc of superconductors, Solid State Commun. **10**, 615 (1972).

[61] P. B. Allen and R. C. Dynes, Transition temperature of strong-coupled superconductors reanalyzed, Phys. Rev. B **12**, 905 (1975).

[62] G. Profeta, C. Franchini, N. N. Lathiotakis, A. Floris, A. Sanna, M. A. L. Marques, M. Lüders, S. Massidda, E. K. U. Gross, and A. Continenza, Superconductivity in Lithium, Potassium, and Aluminum under Extreme Pressure: A First-Principles Study, Phys. Rev. Lett. **96**, 047003 (2006).

[63] M. Rahm, R. Hoffmann, and N. W. Ashcroft, Ternary Gold Hydrides: Routes to Stable and Potentially Superconducting Compounds, J. Am. Chem. Soc. **139**, 8740 (2017).

[64] E. R. Margine and F. Giustino, Anisotropic Migdal-Eliashberg theory using Wannier functions, Phys. Rev. B **87**, 024505 (2013).

[65] Y. Ma, J. S. Tse, T. Cui, D. D. Klug, L. Zhang, Y. Xie, Y. Niu, and G. Zou, First-principles study of electron-phonon coupling in hole- and electron-doped diamonds in the virtual crystal approximation, Phys. Rev. B **72**, 014306 (2005).

[66] P. Hou, F. Belli, R. Bianco, and I. Errea, Strong anharmonic and quantum effects in *Pm*-3*n* AlH_3 under high pressure: A first-principles study, Phys. Rev. B **103**, 134305 (2021).

[67] I. Errea, F. Belli, L. Monacelli, A. Sanna, T. Koretsune, T. Tadano, R. Bianco, M. Calandra, R. Arita, F. Mauri, and J. A. Flores-Livas, Quantum crystal structure in the 250-kelvin superconducting lanthanum hydride, Nature (London) **578**, 66 (2020).

[68] I. Errea, M. Calandra, C. J. Pickard, J. R. Nelson, R. J. Needs, Y. Li, H. Liu, Y. Zhang, Y. Ma, and F. Mauri, Quantum hydrogen-bond symmetrization in the superconducting hydrogen sulfide system, Nature (London) **532**, 81 (2016).

[69] M. Borinaga, U. Aseginolaza, I. Errea, M. Calandra, F. Mauri, and A. Bergara, Anharmonicity and the isotope effect in superconducting lithium at high pressures: A first-principles approach, Phys. Rev. B **96**, 184505 (2017).

[70] J. M. An and W. E. Pickett, Superconductivity of MgB_2: Covalent Bonds Driven Metallic, Phys. Rev. Lett. **86**, 4366 (2001).